New π-arene ruthenium (II) piano-stool complexes with nitrogen ligands

Jordi Grau [a], Verónica Noe [b], Carles Ciudad [b], Maria J. Prieto [c], Mercè Font-Bardia [d], Teresa Calvet [d], Virtudes Moreno [a,*]

[a] Department de Química Inorgànica, Facultat de Química, Universitat de Barcelona, Martí y Franquès 1-11, 08028, Barcelona, Spain

[b] Departament de Bioquímica, Facultat de Farmàcia, Universitat de Barcelona, Diagonal 643, 08028, Barcelona, Spain

[c] Departament de Microbiologia, Facultat de Biologia, Universitat de Barcelona, Diagonal 645, 08028, Barcelona, Spain

[d] Cristal.lografia, Mineralogia i Dipòsits Minerals, Universitat de Barcelona, Martí i Franquès s/n, 08028-Barcelona, Spain

* Corresponding author. Fax: +34 93 4907725.

E-mail address: virtudes.moreno@qi.ub.es (V. Moreno).

Abstract

The synthesis, characterization, DNA interaction and antiproliferative behavior of new π-arene ruthenium(II) piano-stool complexes with nitrogen ligands are described. Three series of organometallic compounds of formulae [$RuCl_2(\eta^6$-p-cym)L] were synthesized (with L=2-, 3- or 4-methylpyridine; L=2,3-, 2,4-, 2,5-, 3,4-, 3,5-dimethylpyridine and L=1,2-, 1,3- 1,4-methylaminobenzene). The crystal structures of [$RuCl_2$(p-cym)(4-methylpyridine)], [$RuCl_2$(p-cym) (3,4-dimethylpyridine)] and [$RuCl_2$(p-cym) (1,4-methylaminobenzene)] were resolved and the characterization was completed by spectroscopic UV–vis, FT-IR and ^{1}H NMR studies. Electrochemical experiments were performed by cyclic voltammetry to estimate the redox potential of the Ru(II)/Ru(III) couple. The interaction with plasmid pBR322 DNA was studied through the examination of the electrophoretical mobility and atomic force microscopy, and interaction with ct-DNA by circular dichroism, viscosity measurements and fluorescence studies based on the DNA–ethidiumbromide complex. The antiproliferative behavior of the series with L=methylpyridine was assayed against two tumor cell lines, i.e. LoVo and MiaPaca. The results revealed a moderate cytotoxicity with a higher activity for the LoVo cell line compared to the MiaPaca one.

1. INTRODUCTION

Since the discovery that cisplatin could inhibit tumor growth, this compound became one of the most widely used anticancer drugs, often as part of the first line of treatment against various tumors [1–3]. However, there are inherent limitations with cisplatin and other platinum compounds (oxaliplatin, carboplatin) in clinical use [4–6], such as their high toxicity that leads to unwanted side effects, and low administration dosage [1,7,8].

These severe drawbacks have initiated the development of new metal-based antitumor drugs; for instance, ruthenium, gold, or osmium compounds have been received much attention in recent years [9]. Hence, ruthenium-based antitumor complexes represent a promising alternative to platinum drugs, a number of them being already in clinical trials [10,11]. Ruthenium has a large range of available oxidation states at physiological conditions. Additionally, Ru(III) compounds are believed to behave as pro-drugs, with low toxicity after activation by reduction to the corresponding Ru(II) compound [12]. Many Ru(III) DMSO complexes, for instance NAMI-A (Imidazolium trans-imidazole dimethyl sulfoxide tetrachlororuthenate) derived compounds, show interesting anti-metastatic activities [13]. Even though the mechanism of action of ruthenium-based drugs is still unclear, it is believed that the ability of ruthenium to mimic iron in the binding to biological molecules (such as transferrin or albumin) is an important feature. This property is mainly reflected in less toxic compounds compared to their platinum counterparts [14], resulting from a more efficient delivery to cancer cells. The mechanism of action seems to be different from that of the platinum compounds, making these ruthenium compounds suitable to circumvent the resistance to platinum molecules developed by several cell lines. Therefore, ruthenium compounds have a great potential as anticancer agents [15], and different approaches of investigation have been reviewed recently [16].

Lately, ruthenium(II) complexes incorporating arene ligands, such as cyclopentadienyl [17,18] or p-cym, exhibiting antitumor activity have been reported [16,19,20]. The most representative compounds of this class, are the so-called piano-stool complexes like RAPTA-C {[Ru(eta(6)-p-cymene)Cl(2) (PTA)]}(PTA=1,3,5-triaza-7-phosphatricyclo-[3.3.1.1] decanephosphine) [21]. This compound possesses metastasis process-inhibiting properties, which are similar to that of NAMI-A at low in vitro anticancer activity [14]. Structural modifications of these organometallic compounds are investigated

currently, to try to establish a possible relationship between their structure and their antitumor activity [22,23].

Most probably, DNA represents the final molecular target for platinum-based cytostatic compounds, giving rise to the inhibition of replication through the creation of crosslinks [24,25]. For ruthenium compounds, their interaction with proteins leading to cell cycle arrest has been evidenced, which is responsible for the activity of NAMI-A [13]; however, the possibility of DNA modifications induced by ruthenium resulting in apoptosis cannot be ruled out. In addition, as shown for KP1019, other cellular targets may be possible as well; for instance, the apoptotic pathway may be provoked by direct interaction with the mitochondrial membrane.

In the present study, eleven new Ru(II) complexes of formula [$RuCl_2(\eta^6$-p-cym)(L)],where L are structural isomers of methylpyridine (A), dimethylpyridine (B) and methylaminobenzene (C) were synthesized and fully characterized, and their potential interactions with DNA were explored. Moreover, competitive binding experiments have been carried out to further investigate their DNAbinding affinities.

2. EXPERIMENTAL

The synthesis of the organometallic complexes [$RuCl_2$(p-cym)(L)] (Scheme 1), where L are structural isomers of methylpyridine (A), dimethylpyridine (B) (Scheme 2), and methylaminobenzene (C), has been carried out according to the method established by Malecki, Jaworski and Kruszynski [26], with slight modifications. The starting material μ-dichloro-[$RuCl_2$(p-cym)]$_2$ was prepared according to a published procedure [25]. All solvents used were purchased from Sigma Aldrich and were of HPLC quality. All organic reagents were obtained from Sigma Aldrich.

FT-IR spectra were recorded as KBr pellets with a Nicolet 5700 FT-IR spectrophotometer. ^{1}H-NMR spectra were recorded on a Varian 300 MHz or Mercury 400 MHz spectrometer at probe temperature. The ^{1}H chemical shifts are reported in parts per million (ppm) downfield from the internal Me_4Si. Elemental analyses were obtained at Recursos Científics de la Universitat Rovira I Virgili, using a Fisons Instruments EA1108 system. Data acquisition, integration and handling were performed using a PC with the software package EAGER-200 (Carlo Erba Instruments). UV–vis studies were obtained with a Varian Cary 100 scan UV–vis spectrophotometrer dual-beam quartz cuvette with an optical path of 1 cm. CH_2Cl_2 was used as blank. Single crystals for X-ray analysis were obtained by slow diffusion of diethyl ether in CH_2Cl_2.

2.1. DNA interaction studies

2.1.1. Circular dichroism

All compounds were dissolved in an aqueous solution (prepared with milli-Q water) containing 2% DMSO (2 mg compound/5 mL). The stock solutions were freshly prepared, just before use. The samples were prepared by addition of aliquots of these stock solutions to the appropriate volume of Calf Thymus DNA in a TE buffer solution (50 mM NaCl, 10 mM tris-(hydroxymethyl)aminomethane hydrochloride (Tris–HCl), 0.1 mM H_4edta, pH 7.4) (5 mL). The amount of complex added to the DNA solution was designated as ri (the input molar ratio of Ru to nucleotide), which is calculated with the formula:

$$ri = \frac{m\ x\ Mnucl\ x\ Am}{C\ x\ Mr\ x\ V}$$

where m = mass of the compound (in μg); M_{nucl} = medium nuclear mass per nucleotide (330 g/mol); C = concentration of the DNA solution (in μg/mL); *Mr* = molecular mass of each compound (g/mol); and *V* = total volume of each sample (5 mL).

As a blank, a solution in TE of free native DNA was used. The CD spectra of DNA in the presence or absence of the complexes (DNA concentration 20 μg/mL, molar ratios ri = 0.10, 0.30, 0.50) were recorded at room temperature, after 24 h incubation at 37 °C, on a JASCO J-720 spectropolarimeter with a 450W xenon lamp using a computer for spectral subtraction and noise reduction. Each sample was scanned twice in a range of wavelengths between 220 and 330 nm. The CD spectra drawn are the average of three independent scans. The data are expressed as average residue molecular ellipticity (θ) in degrees·cm^2·$dmol^{-1}$.

2.1.2. Viscosity measurements

Viscosity experiments were carried out with an AND-SV-1 viscometer in a water bath using a water jacket accessory and maintained at a constant temperature of 25 °C.

All compounds were dissolved in an aqueous solution (prepared with milli-Q water) containing 2% DMSO (1 mg compound/1 mL). The stock solutions were freshly prepared, just before use. The samples were prepared by addition of aliquots of these stock solutions to the appropriate volume of calf thymus DNA in a TE buffer solution (50 mM NaCl, 10 mM tris-(hydroxymethyl)aminomethane hydrochloride (Tris–HCl), 0.1 mM H_4edta, pH 7.4) (5 mL). The amount of complex added to the DNA solution was designated as ri.

As a blank, a solution in TE of free native DNAwas used. The viscosity spectra of DNA in the presence or absence of complexes (DNA concentration 20 μg/mL, molar ratios ri = 0.1 to 0.5) were recorded at 25 °C, after 24 h incubation at 37 °C.

2.1.3. Atomic force microscopy (TMAFM)

A stock solution with concentration 1 mg/mL in a buffer solution of HEPES (4 mM Hepes, pH 7.4/ 2 mM $MgCl_2$) was used. Each sample contained 1 μL of DNA pBR322 of

concentration 0.25 μg/μL for a final volume of 40 μL. The amount of drug added is also expressed as ri. After 3 h of incubation, the AFM samples were prepared by casting a 3-μL drop of test solution onto freshly cleaved Muscovite green mica disks as the supports. The drop was allowed to stand undisturbed for 3 min to favor the adsorbate–substrate interaction. Each DNA-laden disk was rinsed with Milli-Q water and was blown dry with clean compressed argon gas directed normal to the disk surface. Samples were stored over silica prior to AFM imaging. All Atomic Force Microscopy (AFM) observations were made with a Nanoscope III Multimode AFM (Digital Instrumentals, Santa Barbara, CA). Nanocrystalline Si cantilevers of 125-nm length with a spring constant of 50 N/m average ended with conical-shaped Si probe tips of 10-nm apical radius and cone angle of 35° were utilized. High-resolution topographic AFM images were performed in air at room temperature (relative humidity < 40%), on different specimen areas of 2×2 μm^2 operating in intermittent contact mode at a rate of 1–3 Hz.

2.1.4. Gel electrophoresis of ruthenium complexes-pBR322

pBR322 DNA aliquots (0.25 μg/mL) were incubated in TE buffer (10 mM Tris.HCl, 1 mM EDTA, pH = 7.5) at molar ratio ri = 0.50 for electrophoresis study. Incubation was carried out in the dark at 37 °C for 24 h. 4 μL of charge marker was added to aliquots parts of 20 μL of the compound–DNA complex. The mixture was electrophoresed in agarose gel (1% in TBE buffer, Tris–Borate–EDTA) for 5 h at 1.5 V/cm. Afterwards, the DNA was dyed with an ethidium bromide solution (0.75 μg/mL in TBE) for 6 h. A sample of free DNA was used as control. The experiment was carried out in an ECOGEN horizontal tank connected to a PHARMACIA GPS 200/400 variable potential power supply, and the gel was photographed with an image Master VDS, Pharmacia Biotech.

2.1.5. Fluorescence measurements with the DNA–ethidium bromide (EB) complex

All compounds were dissolved in an aqueous solution (prepared with milli-q water) containing 2% DMSO (2 mg compound/5 mL). The stock solutions were freshly prepared, just before use. The samples were prepared by addition of aliquots of these stock solutions to the appropriate volume of calf thymus DNA in a TE buffer solution. The amount of complex added to the DNA solution was designated as ri.

As a blank, a solution in TE of free native DNA and EB was used. The fluorescence spectra of DNA in the presence or absence of complexes (DNA concentration 20 μg/mL, molar ratios ri = 0.1 to 0.5) were recorded at room temperature, after 24 h incubation at 37 °C, on a Nandog™-Horiba Jobin Yvon spectrofluorometer with a 450W xenon lamp using a computer for spectral subtraction and noise reduction. Each sample was scanned twice in a range of wavelengths between 500 and 730 nm, after have been excited at 520 nm.

2.2. Tumor cell lines and culture conditions

LoVo human colon adenocarcinoma and MiaPaCa pancreatic cancer cell lines were used throughout the study. Cells were grown in F-12 medium (Gibco) supplemented with 5% (v/v) fetal bovine serum (Gibco), 100 U/mL sodium penicillin G and 100 μg/mL streptomycin, and were maintained at 37 °C in a humidified atmosphere containing 5% CO2.

2.3. Cytotoxicity assays

Thirty thousand LoVo or MiaPaca cells were seeded in 35mmdiameter dishes in 2 ml of F-12medium. Cells were cultured for 2 h without treatment and then incubated with the different compounds at the indicated concentrations. After 7 days of incubation, cell growth was determined by the MTT test [27]. Briefly, 200 μl of a 0.5 mg/mL MTT solution [3-(4,5-dimethylthiazolyl-2)-2,5-diphenyltetrazolium bromide] (Sigma) and 700 μl of a 50 mM succinic acid solution, both in PBS, were added to each well. The dishes were incubated at 37 °C for 3 h to allow the formation of formazan crystals. Then, the dark blue crystals were dissolved with 10% SDS in DMSO solution and their absorbance was read at 570 nM on a spectrophotometer. Results are expressed as a percentage of survival with respect to the control cells grown in the absence of compounds. IC50 values (drug concentration at which 50% of the cells are viable relative to the control) were obtained by GraphPad Prism software, version 4.0.

2.4. Synthesis of the new complexes

2.4.1. Synthesis of [$RuCl_2$(p-cym)(pic)] (A1, A2, A3)

In a 50mL round-bottom flask, 0.1 g (0.16mmol) of starting material was dissolved in the minimum amount of methanol, and 150 μL (1.92mmol) of the respective methylpyridine was added. The reaction mixture was refluxed (at 65 °C) for about 8 h. In the course of the reaction, a change of color was observed and a yellow precipitate formed. The obtained solid was recrystallized from dichloromethane/diethyl ether.

2.4.1.1. Synthesis of [RuCl2(p-cym)(2-pic)] (A1). Yield: 66%. FT-IR [KBr, cm^{-1}]: C\N (bd) 1615(s); Ru\N(bd): 848 (m); 2-pic (bd): 723 (m). ^{1}H NMR [$CDCl_3$, Me_4Si, δ/ppm]: 2.09 [singlet, 3, CH_3 (p-cym)]; 2.85 [septuplet, 1, CH(p-cym); J=6.9 Hz]; 1.21 [d, 6, isopropyl (p-cym;) J=6.9 Hz]; 5.26-5.43 [dd, 4, H phenyl (p-cym); J=5.1 Hz]; 2.49 [singlet, 3, CH_3(2-pic)]; 7.08-8.43 [m, 4,H (2-pic)]. UV–vis in CH_2Cl_2, λmax/nm (ε/M^{-1} cm^{-1}): d➔d: 418 (148); CT d➔π*pic: 336 (174); CT: πCl\πCl *263 (720); LLCT $\pi_{p\text{-}cym}$➔$\pi^*_{p\text{-}cym}$: 228 (1170). Elem. Anal. Found: C, 47.72; H, 5.16; N, 3.56; Calc. for $C_{16}H_{21}Cl_2NRu$; C, 48.12; H, 5.30; N, 3.51.

2.4.1.2. Synthesis of [RuCl2(p-cym)(3-pic)] (A2). Yield: 58%. FT-IR [KBr, cm^{-1}]: C\N (bd) 1605(s); Ru\N(bd): 855 (s); 3-pic (bd): 723 (m). ^{1}H NMR [$CDCl_3$, Me_4 Si, δ/ppm]: 2.09 [singlet, 3, CH_3 (p-cym)]; 2.98 [septuplet, 1, CH(p-cym); J=6.9 Hz]; 1.31 [d, 6, isopropyl (p-cym;) J=6.9 Hz]; 5.20-5.43 [dd, 4, H phenyl (p-cym); J=5.1 Hz]; 2.45 [singlet, 3, CH_3(3-pic)]; 7.20-8.86 [m, 4, H (3-pic)]. UV–vis in CH_2Cl_2, λ_{max}/nm (ε/M^{-1} cm^{-1}): d➔d: 409 (116); CT d➔π^*_{pic}: 286 (1113); CT: πCl➔π_{Cl}*271 (1134); LLCT: $\pi_{p\text{-}cym}$➔$\pi^*_{p\text{-}cym}$: 230 (1713). Elem. Anal. Found: C, 47.90; H, 5.71; N, 3.28; Calc. for $C_{16}H_{21}Cl_2NRu$; C, 48.12; H, 5.30; N, 3.51.

2.4.1.3. Synthesis of [RuCl2(p-cym)(4-pic)] (A3). Yield: 83%. FT-IR [KBr, cm^{-1}]: C\N $_{(bd)}$ 1615(s); Ru\N$_{(bd)}$: 811 (s); 4-pic $_{(bd)}$: 650 (m). ^{1}H NMR [$CDCl_3$, Me_4Si, δ/ppm]: 2.10

[singlet, 3, CH_3 (p-cym)]; 2.98 [septuplet, 1, CH(p-cym); J=6.9 Hz]; 1.30 [d, 6, isopropyl (p-cym;) J=6.9 Hz]; 5.23-5.47 [dd, 4, H phenyl (p-cym); J=6.0 Hz]; 2.41 [singlet, 3, CH_3(4-pic)]; 7.12-8.85 [dd, 4, H (4-pic); J_{H1-H2}=6, 6 Hz]. UV–vis in CH_2Cl_2, λ_{max}/nm (ε/M^{-1} cm^{-1}): d➔d: 398 (3528); CT d➔π^*_{pic}: 282 (6301); CT: π_{Cl}➔π_{Cl} *263 (7880); LLCT: $\pi_{p\text{-}cym}$➔$\pi^*_{p\text{-}cym}$: 228 (14,389). Elem. Anal. Found: C, 48,75; H, 5.19; N, 3.14; Calc. for $C_{16}H_{21}Cl_2NRu$; C, 48.12; H, 5.30; N, 3.51.

2.4.2. Synthesis of [RuCl2(p-cym)(lut)] (B1, B2, B3, B4, B5)

In a 50 mL round-bottom flask, 0.1 g (0.16 mmol) of starting material was dissolved in the minimum amount of methanol and 150 µL (2,54 mmol) of the corresponding dimethylpyridine were added. The resulting mixture was refluxed (at 65 °C) for about 8 hours. During the course of the reaction, a color change was observed, and a brown oil formed. The brown oily residue was treated with diethyl ether, and a yellow solid was obtained that was recrystallized from dichloromethane/diethyl ether.

2.4.2.1. Synthesis of [RuCl2(p-cym)(2,3-lut)] (B1). Yield: 80%. FT-IR [KBr, cm^{-1}]: C\N (bd) 1592(m); Ru\N(bd): 878 (m); 2,3-lut: 848 (m), 748 (s), 684 (m). ^{1}H NMR [$CDCl_3$, Me_4Si, δ/ppm]: 2.16 [singlet, 3, CH_3(p-cym]; 2.94 [septuplet, 1, CH (p-cym; J=6.8 Hz]; 1.28 [d, 6, isopropyl (p-cym); J=6.8 Hz]; 5.33-5.47 [dd, 4, H phenyl (p-cym); J=5.02 Hz];]; 2.28 [s, 3, CH_{3A}(2.3-lut)]; 2.50 [singlet, 3, CH_{3B}(2.3- lut)]; 7.38-8.33[m, 3, H (2.3-lut)]. UV–vis in CH_2Cl_2, λ_{max}/nm (ε/M^{-1} cm^{-1}): d➔d: 444 (1040); CT d➔π^*_{lut}: 341 (1096); CT: π_{Cl}➔π_{Cl} *266 (4688); LLCT: $\pi_{p\text{-}cym}$➔$\pi^*_{p\text{-}cym}$: 230 (10,180). Elem. Anal. Found: C, 48.95; H, 5.92; N, 3.71; Calc. for $C_{17}H_{23}Cl_2NRu$; C, 49.40; H, 5.61; N, 3.39.

2.4.2.2. Synthesis of [RuCl2(p-cym)(2,4-lut)] (B2). Yield: 23%. FT-IR [KBr, cm^{-1}]: C\N (bd) 1618(s); Ru\N(bd): 884 (m); 2,4-lut: 812 (m), 724 (m), 662 (m). ^{1}H NMR [$CDCl_3$,

266 Me_4Si, δ/ppm]: 2.16 [singlet, 3, CH_3(p-cym]; 2.92 [septuplet, 1, CH (p-cym; J=6.4 Hz]; 1.28
267 [d, 6, isopropyl (p-cym); J=6.4 Hz]; 5.33-5.47 [dd, 4, H phenyl (p-cym); J=4.04 Hz];]; 2.59
268 [s, 3, CH_{3A}(2.4-lut)]; 2.32 [singlet, 3, CH_{3B}(2.4-lut)]; 6.99 [singlet, 1, H_3(2.4-lut)]; 6.93-
269 8.36 [dd, 2, H^1H_2 (2.3-lut)]. UV–vis in CH2Cl2, λ_{max}/nm (ε/M^{-1} cm^{-1}): d➔d: 447 (1168);
270 CT d➔π^*_{lut}: 337 (1211); CT: π_{Cl}➔π_{Cl} *268 (5368); LLCT: $\pi_{p\text{-}cym}$➔$\pi^*_{p\text{-}cym}$: 228 (5750).
271 Elem. Anal. Found: C, 48.67; H, 5.66; N, 3.53; Calc. for $C_{17}H_{23}Cl_2NRu$; C, 49.40; H, 5.61;
272 N, 3.39.
273
274 *2.4.2.3. Synthesis of [$RuCl_2$(p-cym)(2,5-lut)] (B3).* Yield: 82%. FT-IR [KBr, cm^{-1}]: C\N
275 (bd) 1608(m); Ru\N(bd): 888 (m); 2,5-lut: 828 (s), 721 (m), 663 (m). ^{1}H NMR [$CDCl_3$,
276 Me_4Si, δ/ppm]: 2.16 [singlet, 3, CH_3(p-cym]; 2.91 [septuplet, 1, CH (p-cym; J=6.6 Hz]; 1.28
277 [d, 6, isopropyl (p-cym); J=6.6 Hz]; 5.34-5.57 [dd, 4, H phenyl (p-cym); J=5,10 Hz];]; 2,29
278 [singlet, 3, CH_{3A}(2.5-lut)]; 2.53 [singlet, 3, CH_{3B}(2.5-lut)]; 7.07 [singlet, 1, H_1(2.5-lut)]
279 7.74 -8.34 [dd, 2, H_2H_3 (2.5-lut)]. UV–vis in CH_2Cl_2, λ_{max}/nm (ε/M^{-1} cm^{-1}): d➔d: 444
280 (1271); CT d➔π^*_{lut}: 332 (1563); CT: π_{Cl}➔π_{Cl}*270 (10,833); LLCT: $\pi_{p\text{-}cym}$➔$\pi^*_{p\text{-}cym}$:
281 228 (10,427). Elem. Anal. Found: C, 48.41; H, 5.61; N, 3.34; Calc. for $C_{17}H_{23}Cl_2NRu$; C,
282 49.40; H, 5.61; N, 3.39.
283
284 *2.4.2.4. Synthesis of [$RuCl_2$(p-cym)(3,4-lut)] (B4).* Yield: 32%. FT-IR [KBr, cm^{-1}]: C\N
285 (bd) 1609(s); Ru\N(bd): 873 (m); 3,4-lut: 831 (f), 712 (m), 670 (w). ^{1}H NMR [$CDCl_3$,
286 Me_4Si, δ/ppm]: 2.17 [singlet, 3, CH_3(p-cym]; 2.97 [septuplet, 1, CH (p-cym; J=5,1 Hz]; 1.29
287 [d, 6, isopropyl (p-cym); J=5,1 Hz]; 5.21-5.42 [dd, 4, H phenyl (p-cym); J=3,6 Hz];]; 2,33
288 [singlet, 3, CH_{3A}(3,4-lut)]; 2.28 [singlet, 3, CH_{3B}(3,4-lut)]; 8,70 [singlet, 1, H_3 (3,4-lut)]
289 7.19 -9.22 [dd, 2, H^1H_2 (3,4-lut)]. UV–vis in CH_2Cl_2, λ_{max}/nm (ε/M^{-1} cm^{-1}): d➔d: 386
290 (2171); CT d➔π^*_{lut}: 347 (2873); CT: π_{Cl}➔π_{Cl}*268 (11,723); LLCT: $\pi_{p\text{-}cym}$➔$\pi^*_{p\text{-}cym}$:

228 (15,592). Elem. Anal. Found: C, 49.92; H, 6.14; N, 4.42; Calc. for $C_{17}H_{23}Cl_2NRu$; C, 49.40; H, 5.61; N, 3.39.

2.4.2.5. Synthesis of [$RuCl_2$(p-cym)(3,5-lut)] (B5). Yield: 66%. FT-IR [KBr, cm^{-1}]: C\N (bd) 1585 (m); Ru\N(bd): 881 (m); 3,5-lut: 868 (s), 712 (m), 695 (m). ^{1}H NMR [$CDCl_3$, Me4Si, δ/ppm]: 2.14 [singlet, 3, CH_3(p-cym]; 2.98 [septuplet, 1, CH (p-cym; J=6.6 Hz]; 1.29 [d, 6, isopropyl (p-cym); J=6.1 Hz]; 5.29-5.42 [dd, 4, H phenyl (p-cym); J=2.02 Hz];]; 2.33 [singlet, 6, CH_{3A} and CH_{3B} (3.5-lut)]; 7.07 [singlet, 1, H_1(2.5-lut)]; 8.67 [singlet, 1, H_1(3.5-lut)]; 7.34 [singlet, 1, H_2 (3.5- lut)]. UV–vis in CH_2Cl_2, λ_{max}/nm (ε/M^{-1} cm^{-1}): d➔d: 403 (953); CT d➔π^*_{lut}: 330 (1568); CT: π_{Cl}➔$\pi_{Cl}{}^*$275 (8763); LLCT: $\pi_{p\text{-}cym}$➔$\pi^*_{p\text{-}cym}$: 229 (11,882). Elem. Anal. Found: C, 49.89; H, 5.83; N, 3.29; Calc. for $C_{17}H_{23}Cl_2NRu$; C, 49.40; H, 5.61; N, 3.39.

2.4.3. Synthesis of [$RuCl_2$(p-cym)(tol)] (C1, C2, C3)

In a 50 mL round-bottom flask, 0.1 g (0.16 mmol) of starting material was dissolved in the minimum amount of methanol and 150 μL (2,18 mmol) of the respective methylaminobenzene were added. The ensuing reaction mixture was refluxed (at 65 °C) for about 8 hours. During the course of the reaction a color change was observed and an orange oil formed. The orange oily residue was treated with diethyl ether to obtain an orange solid that was recrystallized from dichloromethane/diethyl ether.

2.4.3.1. Synthesis of [$RuCl_2$(p-cym)(o-tol)] (C1). Yield: 63%. FT-IR [KBr, cm^{-1}]: N\H(st): 3228(m), C\N (bd) 1610(m); o-tol: 876 (s), 746 (w), 702 (w). ^{1}H NMR [$CDCl_3$, Me_4Si, δ/ppm]: 2.15 [singlet, 3, CH_3(pcym)]; 2.95 [septuplet, 1, CH(p-cym); J=6.6 Hz]; 1.29 [d, 6, isopropyl (p-eyme); J=6.6 Hz]; 4.83–4.98 [dd, 4, phenyl (p-cym); J=6 Hz]; 2.45 [singlet, 3, CH_3(o-tol)]; 7.11–7.17 [pseudo-singlet, 4, H (o-tol)]; 4.65 [pseudo-singlet, 2, NH_2 (m-tol)].

UV–vis in CH_2Cl_2, λ_{max}/nm ($\varepsilon/M^{-1}\ cm^{-1}$): d➔d: 419 (119); CT d➔$\pi^*_{tol}$: 341 (1789); CT: π_{Cl}➔π_{Cl}^*261 (9382); LLCT: $\pi_{p\text{-}cym}$➔$\pi^*_{p\text{-}cym}$: 228 (15,000). Elem. Anal. Found: C, 49.50; H, 6.05; N, 3.42; Calc, for $C_{17}H_{23}Cl_2NRu$; C, 49.40; H, 5.61; N, 3.39.

2.4.3.2. Synthesis of [$RuCl_2$(p-cym)(m-tol)] (C2). Yield: 71%. FT-IR [KBr, cm^{-1}]: N\H(st): 3196(m), C\N (bd) 1602(s); m-tol: 878 (s), 785 (w), 692 (w). ^{1}H NMR [$CDCl_3$, Me_4Si, δ/ppm]: 2.15 [singlet, 3, CH_3(pcym)]; 2.95 [septuplet, 1, CH(p-cym); J=6.6 Hz]; 1.25 [d, 6, isopropyl (p-cym); J=6.6 Hz]; 4.93–4.97 [dd, 4, phenyl (p-cym); J=6 Hz]; 2.39 [singlet, 3, CH_3(m-tol)]; 6.,84–7.11 [pseudo-singlet, 4, H (m-tol)]; 4.68 [pseudo-singlet, 2, NH_2(m-tol)]. UV–vis in CH_2Cl_2, λ_{max}/nm ($\varepsilon/M^{-1}\ cm^{-1}$): d➔d: 415 (957); CT d➔$\pi^*_{tol}$ 340 (1638); LLCT: π_{Cl}➔π_{Cl} * 265 (10,155); CT: $\pi_{p\text{-}cym}$➔$\pi^*_{p\text{-}cym}$: 228 (11,820). Elem. Anal. Found: C, 49.20; H, 5.66; N, 3.59; Calc, for $C_{17}H_{23}Cl_2NRu$; C, 49.40; H, 5.61; N, 3.39.

2.4.3.3. Synthesis of [$RuCl_2$(p-cym)(p-tol)] (C3). Yield: 67%. FT-IR [KBr, cm^{-1}]: N\$H_{(st)}$: 3206(s), C\N $_{(bd)}$ 1612(m); p-tol: 878 (s), 737 (w), 703 (w). ^{1}H NMR [$CDCl_3$, Me_4Si, δ/ppm]: 2.15 [singlet, 3, CH_3(pcym)]; 2.91 [septuplet, 1, CH(p-cym); J=6.4 Hz]; 1.26 [d, 6, isopropyl (p-cym); J=6.4 Hz]; 4.95–5.02 [dd, 4, phenyl (p-cym); J=4.98 Hz]; 2.36 [singlet, 3, CH_3(p-tol)]]; 6.,84–7.11 [pseudo-singlet, 4, H (ptol)]; 4.67 [pseudo-singlet, 2, NH_2 (p-tol)]. UV–vis in CH_2Cl_2, λ_{max}/nm ($\varepsilon/M^{-1}\ cm^{-1}$): d➔d: 412 (1214); CT d➔π^*_{tol} 341 (2143); LLCT: π_{Cl}➔π_{Cl} * 266 (10,780); LLCT: $\pi_{p\text{-}cym}$➔$\pi^*_{p\text{-}cym}$: 229 (86,000). Elem. Anal. Found: C, 50.22; H, 6.07; N, 3.95; Calc, for $C_{17}H_{23}Cl_2NRu$; C, 49.40; H, 5.61; N, 3.39.

2.5. Crystal structure determination

A prismatic crystal (0.1×0.1×0.2 mm^3) was selected and mounted on a MAR345 diffractometer with an image plate detector. Unit-cell parameters were determined from 6582 reflections ($3< \theta <21°$) and refined by least-squares method. Intensities were collected with graphite monochromatized Mo Kα radiation. 32,691 reflections were measured in the range $1.70 \leqslant \theta \leqslant 32.28$. 7222 of which were non-equivalent by symmetry (R_{int}(on I) = 0.062). 7163 reflections were assumed as observed applying the condition $I > 2\sigma(I)$. Lorentz-polarization and absorption corrections were made.

The structure was solved by Directmethods, using SHELXS computer program (Sheldrick, G.M., (1997), a program for automatic solution of crystal structure. University of Goettingen. Germany) and refined by full-matrix least-squares method with SHELX97 computer program (Sheldrick, G.M., (1997). A program for crystal structure refinement, University of Goettingen, Germany), using 7222 reflections, (very negative intensities were not assumed). The function minimized was Σ w $||F_o|^2-|F_c|2$ |2, where $w = [\sigma^2(I)+(0.0300P)^2+67.6165P]^{-1}$, and $P = (|F_o|^2+2\ |F_c|^2\ )/3$, f, f′ and f″ were taken from International Tables of X-Ray Crystallography (International Tables of X-Ray Crystallography, (1974), Ed. Kynoch press, Vol. IV, pp 99–100 and 149). All H atoms were computed and refined, using a riding model, with an isotropic temperature factor equal to 1.2 times the equivalent temperature factor of the atom which is linked. The final *R* (on *F*) factor was 0.062, *wR* (on $|F|^2$) = 0.157 and goodness of fit=1.245 for all observed reflections. Number of refined parameters was 370. Max. shift/esd=0.00, Mean shift/esd=0.00. Max. and min. peaks in final difference synthesis were 1.548 and −1.103 $Å^{-3}$, respectively. CCDC 845858–845860 contain the supplementary crystallographic data for this paper. These data can be obtained free of charge from the Cambridge Crystallographic Data Centre via www.ccdc.cam.ac.uk/data@request/cif.

2.6. Electrochemical experiments

Cyclic voltammograms of ligands and complexes were obtained using a Potentiostat/Galvanostat SP-150 monitored with a personal computer loaded with Electrochemistry PowerSuite v5.31 software from Princeton Applied Research at room

372 temperature. A threeelectrode configuration small capacity cell was equipped with a
373 platinum-disk working electrode (1.0 mm diameter), a carbon electrode as a working
374 electrode and a platinum wire auxiliary electrode. The electrochemical experiments were
375 performed in 0.2 M solutions of $TBAPF_6$ in acetonitrile, under a nitrogen atmosphere, and
376 the redox potentials were measured using ferrocene as the internal standard. The redox
377 potential values were quoted relative to the SCE by using the ferrocenium/ferrocene redox
378 couple [28].

379

380

381

3. RESULTS AND DISCUSSION

3.1. Spectroscopic studies

The eleven compounds prepared have been characterized spectroscopically. The FT-IR spectra exhibit the typical bands of the p-cym and aromatic rings in the region 3040–3080 cm^{-1}. The $\gamma_{C=N}$ band is observed around 1610 cm^{-1}, and the bands characterizing the Ru\Cl and Ru\N_{sp^2} bonds are present at lower wavelength. The ^1H NMR spectra illustrate a downfield chemical shift of the aromatic protons belonging to the p-cym moiety, which is ascribed to the π-bonding of the ligand to the metal center. Interestingly, the compounds of type C shows one signal at 4.65 ppm, corresponding to two protons and that is attributed to the NH_2 protons of aminobenzene units. The UV–vis spectra display four bands in the visible region, whose assignments have been performed using information reported in the literature for similar compounds [26,29]. The transitions above 400 nm are due to d→d transitions. The bands observed between 350 and 260 nm correspond to the MLCT and LMCT transitions, respectively. The higher energy transitions at 228 nm are attributable to LLCTs (inter and intraligand).

3.2. Crystallographic studies

Crystalline materials have been obtained by slow diffusion of diethyl ether into CH_2Cl_2 solutions of the compounds. Single crystals, suitable for X-ray diffraction analysis, were obtained for compounds A3, B4 and C3. The analyses of the data collected reveal that complex A3 crystallizes in the orthorhombic space group Pbna, B4 in the monoclinic space group $P2_{1/n}$ and C3 in the monoclinic space group $P2_{1/c}$ (Table 1 and Fig. 3).

In the three compounds, the ruthenium atom is π-coordinated to the arene p-cymene and the other three positions are distributed between the two chloride ligands and the respective N-ligand, i.e. methylpyridine, dimethylpyridine and aminomethylpyridine, generating “piano stool” complexes, which are typical for such family of compounds (Fig. 1). The deviations from the ideal piano stool for these compounds are minor. The Ru – N and Ru – Cl bond lengths and N – Ru – Cl angles (Table S1, Supplementary material) are

410 comparable to those found for related compounds in the literature [26,29–32]. π-Stacking
411 interactions are noticed between complex molecules A3, which involve the nitrogen ligand.

412

413 *3.3. Electrochemical studies*

414 The electrochemical properties of the ligands and the new Ru(II) complexes have
415 been examined by cyclic voltammetry in acetonitrile solutions (1×10^{-3} M), using 0.2 M
416 tetrabutylammonium hexafluoridophosphate ($TBAPF_6$) as supporting electrolyte. The redox
417 potentials measured at a scan rate of 0.2 V/s are reported in Table 2.

418 All complexes show a comparable voltammetric behavior in acetonitrile. Two metal-
419 centered voltammetric responses are observed, as previously reported for analogous Ru-p-
420 cym-neutral complexes [30]. A well-defined wave at around 1.10 to 1.30 V, corresponding
421 to a quasi-reversible process and involving a one-electron transfer, can be assigned to the
422 oxidation of Ru^{II} to Ru^{III}. On the other hand, complexes of types B and C undergo a second
423 irreversible oxidation between 0.92 and 1.10 V, ascribed to the amino group. These
424 oxidations disappear after successive scans. The corresponding peak potentials are almost
425 identical for all studied complexes and the changes in oxidation potentials most likely arise
426 from the relative stabilization of ruthenium(II) over ruthenium(III) through a combination
427 of σ and π effects due to the ligands.

428

429 *3.4. Biological studies*

430 *3.4.1. Circular dichroism (CD)*

431 CD spectroscopy is a useful technique in analyzing morphologic changes of DNA
432 during drug–DNA interactions. The CD signals are indeed quite sensitive to the different
433 ways DNA can interact with small molecules [33]. A solution of ct-DNA exhibits a positive
434 band due to base stacking and a negative band due to the right-handed helicity of DNA. The
435 changes of the CD signal observed upon DNA interaction with drugs may often be assigned
436 to specific modifications of the DNA structure [34]. Circular dichroism spectra of some
437 selected compounds, one for each series, at several ruthenium complex: DNA molar ratio
438 are depicted in Fig. 2 (a–c). After 24 h of incubation at 37 °C, some changes of molar
439 ellipticity can be observed for the complexes. These alterations in wavelength and ellipticity

(compared to free DNA) indicate modifications on the secondary structure of DNA, resulting from its interaction with the different complexes. These interactions may be covalent in nature, subsequent to the hydrolysis of the two chlorido ligands, and due to the great affinity of the ruthenium (II) for the N positions of the nueclobases, mainly N7 of the guanine.

3.4.2. Atomic force microscopy (AFM)

AFM pictures of free DNA pBR322, and incubated with the complexes A, B, and C are shown in Figs. 3–5. The objective was not to establish quantitative measurements of the changes observed in plasmid pBR322 DNA but to visualize the small changes produced by the complexes upon binding to DNA. Such an experiment is expected to reveal whether or not DNA may be one of the possible

targets of the ruthenium complexes (also in addition to the many potential protein binding sites). Hence, the AFM images, obtained using in vitro conditions, clearly show that the complexes are able to bind DNA and modify its structure, with subsequent dramatic consequences for the cells. The mode of binding of the complexes cannot be elucidated using solely this technique. Complementary studies are necessary to better understand how the interaction between the metal complex and DNA takes place.

The AFM images (Fig. 3) corresponding to DNA incubated with compounds A1, A2 and A3 show modifications of the initial DNA form to supercoiled DNA and to DNA exhibiting kinks. In the images 3b) and 3d) corresponding to complexes A1 and A3, respectively, some DNA strands appear to be cleaved, indicating a slight nuclease effect.

The compounds containing dimethylpyridine ligands, i.e. compounds of type B, strongly interact with DNA, particularly complexes B3 and B4 whose AFM images are shown in Fig. 4. In the case of compound B3, important compact forms of DNA are noted (see Fig. 4a). Compound B4 induces a strong DNA supercoiling (see Fig. 4b). No nuclease effects were observed with this series of Ru complexes. It has to be noted that the incubation conditions applied (concentration, temperature and time) were the same to those for the series A.

Finally, the complexes bearing methylaminobenzene ligands, namely complexes of type C, exhibit a behavior similar to that of two complexes of the A series, since they are

capable of cutting the DNA strands (Fig. 5), therefore acting as nucleases although kinks, compaction and supercoiling can be observed as well.

In summary, these qualitative AFM studies clearly indicate that all eleven compounds interact with DNA. To further confirm this interaction and to try to appraise the mode of interaction, additional techniques were used.

3.4.3. Electrophoretic mobility

The ability of the compounds to modify the tertiary structure of DNA has been evaluated via the potential alteration of the electrophoretic mobility of the covalently closed circular (CCC) and open forms (OC) of pBR322 plasmid DNA. Figures S1 and S2 (Supplementary Material) show the electrophoretic mobilities after incubation with the compounds of types A (lines 1–3) and B (lines 6–10). The mobility of native pBR322 plasmid DNA is shown in lines 4 and 5, and that of plasmid DNA incubated with cisplatin in line 11.

The comparison of the gel electrophoretic mobilities of pBR322 plasmid and the DNA/ruthenium adducts reveals slight modifications of the tertiary structure of DNA induced by the metal-containing compounds. In Figure S1, new bands are observed for the ruthenium complexes of type A (lines 1–3), indicating the presence of additional DNA forms before the OC region. The action of compound B5 (line 10) produces alterations of the gel mobilities of the OC and CCC forms. The two typical bands characterizing coalescence induced by cisplatin are clearly seen in line 11.

Figure S2, illustrates the DNA electrophoretic mobility in the presence of the compounds of type C (lines 2–4). Free pBR322 plasmid DNA and incubated with cisplatin are shown as references in lines 1, 5 and 6, respectively. The mobilities observed for the DNA/ruthenium adducts are in agreement with the fragmentations detected by AFM (see Fig. 5).

3.4.4. Viscosity measurements

DNA is a polyanion; hence, in solution, the negative charges of the phosphate groups unfold the DNA molecule into a more extended form. When metal complexes bind to DNA

500 by means of electrostatic or covalent interactions, a folding of the DNA double helix occurs,
501 producing its shortening, and a decrease of the DNA viscosity. Plots of the cube root of η/η^0
502 (where η is the viscosity of each DNAcomplex solution and η^0 represents the viscosity of
503 the native DNA solution, measured after 24 h incubation at 37 °C) versus ri (molar ratio) are
504 depicted in Fig. 6 (a, b, c). The data illustrate a diminution of the viscosity when ri increases,
505 thus discarding an intercalating interaction. Similar features are observed with all the ligands
506 used. Additional time-dependent viscosity measurements at constant temperature show a
507 decrease of the viscosity, which is indicative of the formation of a covalent bond between
508 the DNA base pairs and the metal ions.

509

510 *3.4.5. Fluorescence studies using the DNA–ethidium bromide (EB) complex*

511 To further investigate the binding mode of the Ru(II) complexes, competitive binding
512 experiments have been carried out. The fluorescence emission of EB (5 mM) bound to DNA
513 (50 μM) in the absence and in the presence of the complexes (after 24 h of incubation) have
514 been recorded, and the results are shown in Fig. 7. Ethidium bromide (EB) is a planar
515 conjugated molecule, whose fluorescence intensity is very weak; however, the fluorescence
516 greatly increases when EB is specifically intercalated between the base pairs of double-
517 stranded DNA. Therefore, EB can be used to probe the interactions between DNA and
518 potential intercalating molecules [35]. The ruthenium complexes herein presented do not
519 show appreciable fluorescence properties in the spectral region studied, in the presence of
520 DNA or not. Moreover, these compounds do not quench the fluorescence of EB in the
521 absence of DNA, under the experimental conditions applied. The intensity of the emission
522 band of the DNA–EB pair at 602 nm increases with the concentration of the Ru (II)
523 complexes after 24 h of incubation. Since intercalated EB is the sole fluorescent species, the
524 fluorescence increase noted suggests that the Ru (II) complexes most likely induce a
525 contraction along the helix axis of DNA. Such a characteristic change is often observed for
526 non-intercalative DNA interactions [36]. The action of complex C1 results in the largest
527 intensity increase (Fig. 7). This feature is consistent with the corresponding data obtained by
528 viscosity measurements (see above), indicating that the DNA/Ru interactions are mostly
529 covalent.

530

3.4.6. Cytotoxicity of the ruthenium complexes against MiaPaca and LoVo cells

The potential cytotoxic effects of the ruthenium complexes have been examined on human pancreas cancer cells (MiaPaca) and colon cancer cells (LoVo), using the MTT assay, which consists of a colorimetric determination of cell viability during in vitro treatment with a drug. The assay, developed as an initial stage of drug screening, measures the amount of MTT reduction by mitochondrial dehydrogenase and assumes that cell viability (corresponding to the reductive activity) is proportional to the production of purple formazan that is measured spectrophotometrically. A low IC_{50} is desired and implies cytotoxicity or anti-proliferation at low drug concentrations. The compounds [$RuCl_2$(*p*-cym)(2-pic)] A1, [$RuCl_2$(*p*-cym)(3-pic)] A2, [$RuCl_2$(*p*-cym)(4-pic)] A3, [$RuCl_2$(*p*-cym)(o-tol)] C1, [$RuCl_2$ (*p*-cym)(m-tol)] C2 and [$RuCl_2$ (*p*-cym)(p-tol)] C3 have been evaluated using this biological test. For this purpose, cells have been exposed to each compound continuously for 24 h, and then assayed for growth using the MTT endpoint assay. The IC_{50} values of complexes A1, A2, and A3, for the growth inhibition of MiaPaca and LoVo cells are summarized in Table 3. The cytotoxic properties of complexes of type C could not be estimated because these compounds are poorly soluble under the experimental conditions required for these trials. All ruthenium complexes investigated in the present study show activities against MiaPaca cells (human pancreas cancer cells) and LoVo cells (colon cancer cells) Complex A3 exhibits the best activity with LoVo cells (Table 3). These values are on the same order of magnitude as those reported for many ruthenium compounds with other types of colon carcinoma cells, [37] but lower than those obtained with other organometallic p-cymene-ruthenium complexes against ovarian cancer cells. The presence of thiophenolato [38] or phosphino [39] ligands improves the cytotoxic properties of π-arene or π-cyclopentadiene ruthenium compounds, with IC50 values in the nanomolar range.

4. CONCLUSION

In summary, eleven new Ru(II) complexes of general formula [RuCl2(p-cym)(L)], where L represents structural isomers of methylpyridine, dimethylpyridine and methylaminobenzene have been synthesized and characterized successfully. Their potential interaction with DNA has been studied and the different investigations carried out have revealed strong changes in the secondary structure of DNA (circular dichroism), as well as in its tertiary structure (gel electrophoretic mobility). Emission spectral studies and viscosity measurements indicate that these complexes interact with ct-DNA through a covalent binding mode. Finally, the complexes of type A exhibit interesting in vitro cytotoxic properties against MiaPaca and LoVo cells.

Abbreviations

A1	[RuCl2(p-cym)(2-pic)]
A2	[RuCl2(p-cym)(3-pic)]
A3	[RuCl2(p-cym)(4-pic)]
B1	[RuCl2(p-cym)(2,3-lut)]
B2	[RuCl2(p-cym)(2,4-lut)]
B3	[RuCl2(p-cym)(2,5-lut)]
B4	[RuCl2(p-cym)(3,4-lut)]
B5	[RuCl2(p-cym)(3,5-lut)]
C1	[RuCl2(p-cym)(o-tol)]
C2	[RuCl2(p-cym)(m-tol)]
C3	[RuCl2(p-cym)(p-tol)]
AE	Elemental Analysis
AFM	Atomic Force Microscopy
CCC	Covalently closed circular pBR322 plasmid DNA
CT	Charge transfer
ct-DNA	Calf Thymus DNA
DC	Circular Dichroism

d➔d	d-d transition
EB E	thidium bromide
HEPES	4-(2-hydroxyethyl)-1-piperazineethanesulfonic acid
lut	Dimethylpyridine
MLCT	Metal-to-ligand charge transfer
LMCT	Ligand-to-metal charge transfer
LLCT	Ligand-to-ligand charge transfer
OC	Open forms pBR322 plasmid DNA
pic	Methylpyridine
TBAPF6	Tetrabutylammonium hexafluoridophosphate
TE	(50 mM NaCl, 10 mM tris-(hydroxymethyl)aminomethane hydrochloride (Tris–HCl), 0.1 mM H4edta, pH 7.4).
tol	methylaminobenzene
TMS	Tetramethylsilane

5. ACKNOWLEDGEMENTS

This work was supported by funding from the Spanish Ministerio de Ciencia e Innovación (CTQ2008-02064). The authors thank Dr. Patrick Gamez for his assistance.

633 # 6. REFERENCES

634 [1] T. Boulikas, M. Vougiouka, Oncol. Rep. 10 (2003) 1663–1682.

635 [2] M. Galanski, V.B. Arion, M.A. Jakupec, B.K. Keppler, Curr. Pharm. Des. 9 (2003)
636 2078–2089.

637 [3] E. Wong, C.M. Giandomenico, Chem. Rev. 99 (1999) 2451–2466.

638 [4] R.A. Alderden, M.D. Hall, T.W. Hambley, J. Chem. Educ. 83 (2006) (728-null).

639 [5] J. Reedijk, Eur. J. Inorg. Chem. 2009 (2009) 1303–1312.

640 [6] J. Fischer, C.R. Ganellin, Analogue-Based Drug Discovery II, Wiley-VCH,
641 Weinheim, 2006 pp 385–394.

642 [7] R. Agarwal, S.B. Kaye, Nat. Rev. Cancer 3 (2003) 502–516.

643 [8] M.A. Fuertes, C. Alonso, J.M. Pérez, Chem. Rev. 103 (2003) 645–662.

644 [9] P.C. Bruijnincx, P.J. Sadler, Curr. Opin. Chem. Biol. 12 (2008) 197–206.

645 [10] C.G. Hartinger, S. Zorbas-Seifried, M.A. Jakupec, B. Kynast, H. Zorbas, B.K.
646 Keppler, J. Inorg. Biochem. 100 (2006) 891–904.

647 [11] J.M. Rademaker-Lakhai, D. van den Bongard, D. Pluim, J.H. Beijnen, J.H. Schellens,
648 Clin. Cancer Res. 10 (2004) 3717–3727.

649 [12] C.S. Allardyce, A. Dorcier, C. Scolaro, P.J. Dyson, Appl. Organomet. Chem. 19
650 (2005) 1–10.

651 [13] E. Alessio, G. Mestroni, A. Bergamo, G. Sava, Curr. Top. Med. Chem. 4 (2004) 1525–
652 1535.

653 [14] P.J. Dyson, G. Sava, Dalton Trans. (2006) 1929–1933.

654 [15] A.H. Velders, H. Kooijman, A.L. Spek, J.G. Haasnoot, D. de Vos, J. Reedijk, Inorg.
655 Chem. 39 (2000) 2966–2967.

656 [16] W.H. Ang, P.J. Dyson, Eur. J. Inorg. Chem. 2006 (2006) 3993.

657 [17] V. Moreno, M. Font-Bardia, T. Calvet, J. Lorenzo, F.X. Aviles, M. H. Garcia, T.S.
658 Morais, A. Valente, M.P. Robalo, J. Inorg. Biochem. 105 (2011) 241–249.

659 [18] V. Moreno, J. Lorenzo, F.X. Aviles, M.H. Garcia, J.P. Ribeiro, T.S. Morais, P.

660 Florindo, M.P. Robalo, Bioinorg. Chem. Appl. 2010 (2010) 11, Article ID 936834.

661 [19] Y.K. Yan, M. Melchart, A. Habtemariam, P.J. Sadler, Chem. Commun. (Camb.)
662 (2005) 4764–4776.

663 [20] G. Süss-Fink, Dalton Trans. 39 (2010) 1673–1688.

664 [21] W.H. Ang, E. Daldini, C. Scolaro, R. Scopelliti, L. Juillerat-Jeannerat, P.J. Dyson,
665 Inorg. Chem. 45 (2006) 9006–9013.

666 [22] M. Hanif, S.M. Meier, W. Kandioller, A. Bytzek, M. Hejl, C.G. Hartinger, A.A.
667 Nazarov, V.B. Arion, M.A. Jakupec, P.J. Dyson, B.K. Keppler, J. Inorg. Biochem. 105
668 (2011) 224–231.

669 [23] A.K. Renfrew, A.D. Phillips, A.E. Egger, C.G. Hartinger, S.S. Bosquain, A.A.
670 Nazarov, B.K. Keppler, L. Gonsalvi, M. Peruzzini, P.J. Dyson, Organometallics 28
671 (2009) 1165–1172.

672 [24] Y.P. Ho, S.C. Au-Yeung, K.K. To, Med. Res. Rev. 23 (2003) 633–655.

673 [25] B. Lippert, Cisplatin: Chemistry and Biochemistry of a Leading Anticancer drugEd,
674 Verlag Helvetica Chimica Acta, Wiley-VCH, Zürich-Weinheim; New York, 1999.

675 [26] J.G. Malecki, M. Jaworska, R. Kruszynski, Polyhedron 25 (2006) 2519–2524.

676 [27] T. Mosmann, J. Immunol. Methods 65 (1983) 55–63.

677 [28] N.G. Connelly, W.E. Geiger, Chem. Rev. 96 (1996) 877–910.

678 [29] I. Bratsos, D. Urankar, E. Zangrando, P. Genova-Kalou, J. Kosmrlj, E. Alessio, I.
679 Turel, Dalton Trans. 40 (2011) 5188–5199.

680 [30] K.N. Kumar, G. Venkatachalam, R. Ramesh, Y. Liu, Polyhedron 27 (2008) 157–166.

681 [31] U. Beck, W. Hummel, H.B. Buergi, A. Ludi, Organometallics 6 (1993) 20.

682 [32] F.B. McCormick, D.D. Cox, W.B. Gleason, Organometallics 12 (1993) 610–612.

683 [33] V.I. Ivanov, L.E. Minchenkova, A.K. Schyolkina, A.I. Poletayev, Biopolymers 12
684 (1973) 89–110.

685 [34] P. Lincoln, E. Tuite, B. Nordén, J. Am. Chem. Soc. 119 (1997) 1454–1455.

686 [35] J.B. LePecq, C. Paoletti, J. Mol. Biol. 27 (1967) 87–106.

[36] T. Biver, F. Secco, M.R. Tine, M. Venturini, J. Inorg. Biochem. 98 (2004) 33–40.

[37] M. Mendoza-Ferri, C.G. Hartinger, R.E. Eichinger, N. Stolyanova, K. Severin, M.A. Jakupec, A.A. Nazarov, B.K. Keppler, Organometallics 27 (2008) 2405–2407.

[38] M. Gras, B. Therrien, G. Süss-Fink, O. Zava, P.J. Dyson, Dalton Trans. 39 (2010) 10305–10313.

[39] M.H. García, T.S. Morais, P. Florido, M.F.M. Piedade, V. Moreno, C. Ciudad, V. Noe, J. Inorg. Biochem. 103 (2009) 354–361.

708 **Table 1** Crystallographic unit cell data for compounds A3, B4 and C3.

709

Unit cell dimension	A3	B4	C3
Crystal system	Orthorhombic	Monoclinic	Monoclinic
Space group	*P*bna	$P2_1/n$	$P2_1/c$
a	12.934 (6) Å	13.435 (4) Å	8.954 (4) Å
b	16.256 (6) Å	7.963 (2) Å	12.387 (3) Å
c	31.989 (11) Å	15.921 (3) Å	17.863 (5) Å
α	90°	90°	90°
β	90°	95.49 (2)°	119.30 (2)°
γ	90°	90°	90°

710

711

712

713 **Table 2.** Cyclic voltammetric data for the [$RuCl_2(\eta^6$-p-cym)(L)] complexes. Supporting
714 electrolyte: $TBAPF_6$ (0.2M); complex concentration: 0.1M; Solvent: MeCN; $\Delta E_p = E_{pa} -$
715 E_{pc} where, E_{pa} and E_{pc} are the anodic and cationic potentials, respectively; $E_{1/2} =$
716 $0.5(E_{pa}+E_{pc})$; Scan rate: 100 mV·s−1.

717

Complexes	E_{pa} (V)	E_{pc} (V)	$E_{1/2}$ (V)	ΔE_p (mV)
A1	1.13	0.92	1.025	210
A2	1.12	1.02	1.07	100
B1	1.29	0.99	1.14	300
	1.01	–	–	–
B3	1.21	1.01	1.11	200
	0.92	–	–	–
B5	1.11	1.01	1.06	100
	0.96	–	–	–
C1	1.24	1.11	1.175	130
	0.89	–	–	–
C2	1.18	1.05	1.115	130
	0.78	–	–	–
C3	1.27	1.05	1.16	220
	0.81	–	–	–

718

719

720

721

722 **Table 3** IC50 values obtained with complexes [$RuCl_2$(p-cym)(2-pic)] A1, [$RuCl_2$(p-cym)(3-
723 pic)] A2 and [$RuCl_2$(p-cym)(4-pic)] A3.

724

complex	IC_{50} (μM) MiaPaca cells (24 h)	IC_{50} (μM) LoVo cells (24 h)
[$RuCl_2(\eta^6$-*p*-cym)(*2*-pic)] A1	258	78
[$RuCl_2(\eta^6$-p-cym)(*3*-pic)] A2	155	90
[$RuCl_2(\eta^6$-p-cym)(*4*-pic)] A3	240	>50

725

726

727

728

Figures Captions

Scheme 1. Reaction scheme for the synthesis of the organometallic compounds. L symbolizes structural isomers of methylpyridine (A), dimethylpyridine (B) and methylaminobenzene (C).

Scheme 2. Representation of the dimethylpyridine ligands with the corresponding proton labelings used for the ^{1}H-NMR assignments. a) ligand 2,3-dimethylpyridine, b) 2,4-dimethylpyridine c) 2,5-dimethylpyridine d) 3,4-dimethylpyridine and e) 3,5-dimethylpyridine.

Figure 1. Representation of the single-crystal X-ray structures of complexes a) A3, b) B4 and c) C3.

Figure 2. Circular dichroism spectra of ct-DNA incubated at 37 °C for 24 h with the complexes at molar ratios ri = 0.1, 0.3 and 0.5. a) Complex A2, b) complex B4 and c) complex C2.

Figure 3. AFM images of a) free plasmid pBR322 DNA; b) plasmid pBR322 DNA incubated with complex A1; c) complex A2; d) complex A3 at molar ratio ri = 0.5.

Figure 4. AFM images of a) plasmid pBR322 DNA incubated with complex B3 and b) complex B4 at molar ratio ri =0.5.

Figure 5. AFM images of a) plasmid pBR322 DNA incubated with complex C1 and b) complex C2 at molar ratio ri=0.5.

Figure 6. Plots of $(\eta/\eta^{0})^{(1/3)}$ (where η is the viscosity of each DNA-complex solution and η^{0} is the viscosity of the native DNA solution, measured after 24 h incubation at 37 °C) versus ri (molar ratio) for a) complexes of type A, b) complexes of type B, c) complexes of type C.

Figure 7. Fluorescense spectra of ct-DNA incubated with complex C1 at different concentrations (10, 20, 30, 40 and 50 mM), at 37 °C for 24 h.

759 **Scheme 1.**

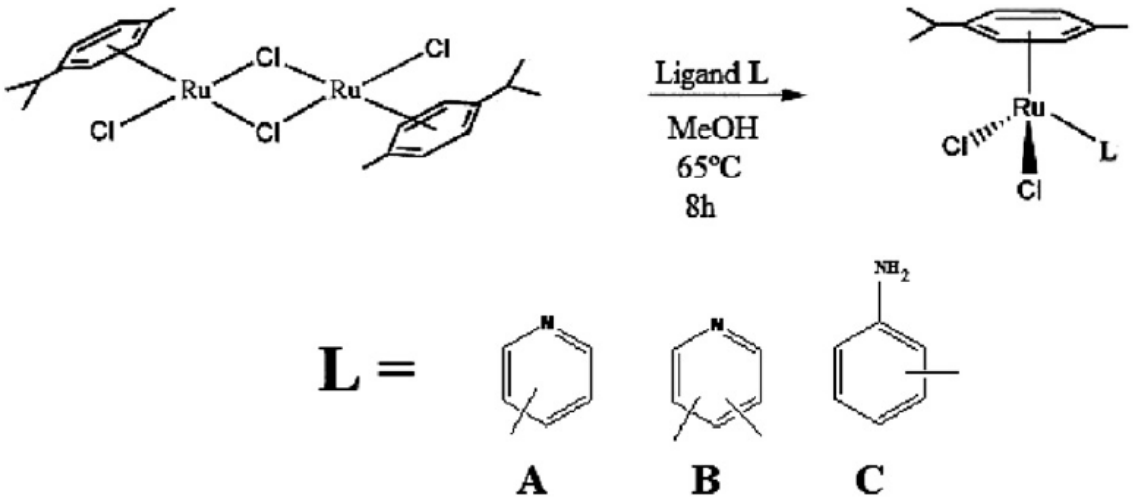

760

761

762

763 **Scheme 2**

764

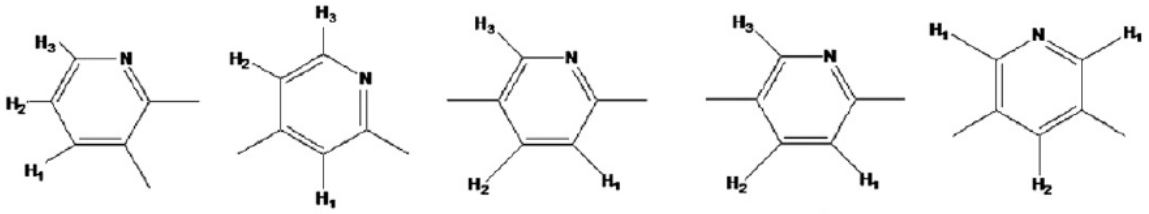

765

766

767

768

769 **Figure 1**

770

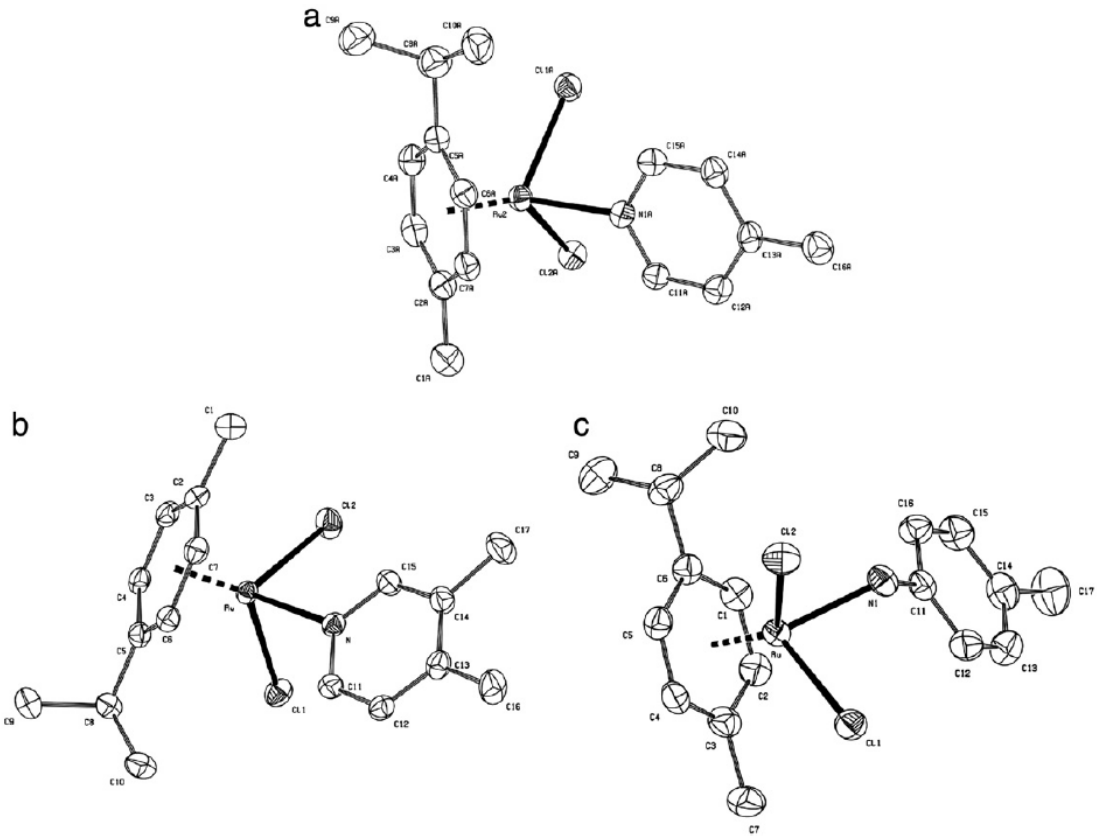

771

772

773

774

775 **Figure 2**

776

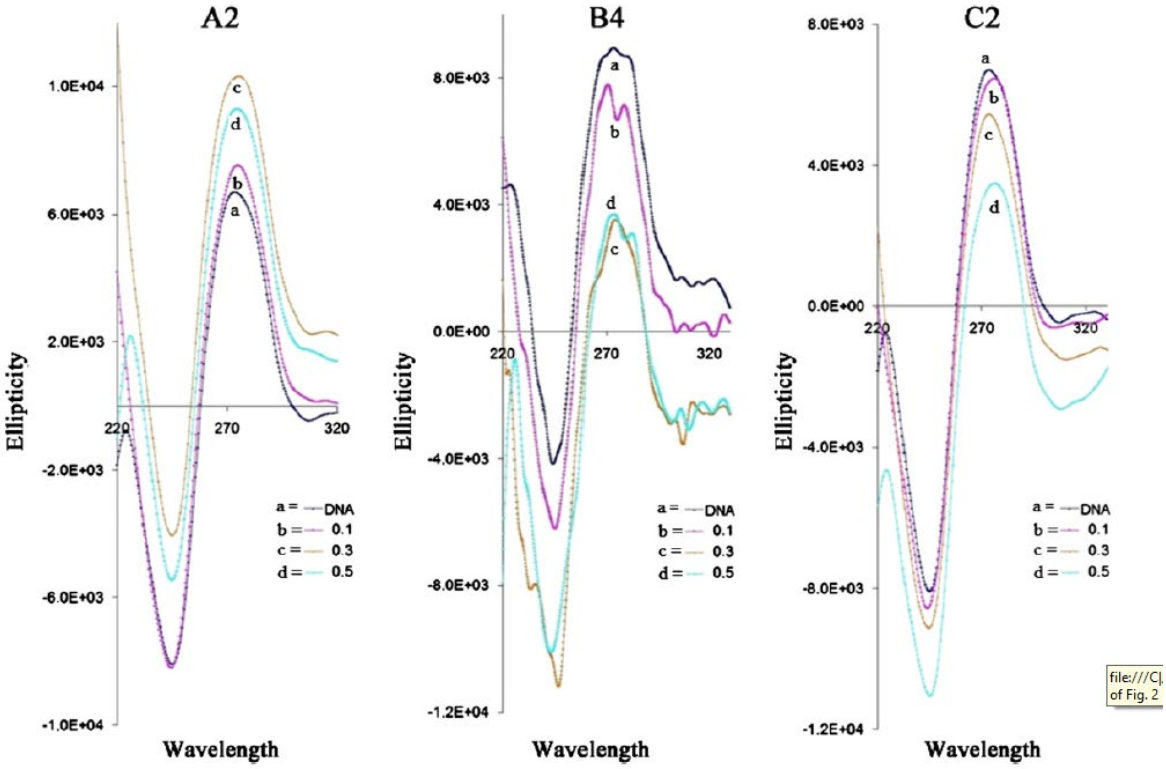

777

778

779

780 **Figure 3**

781

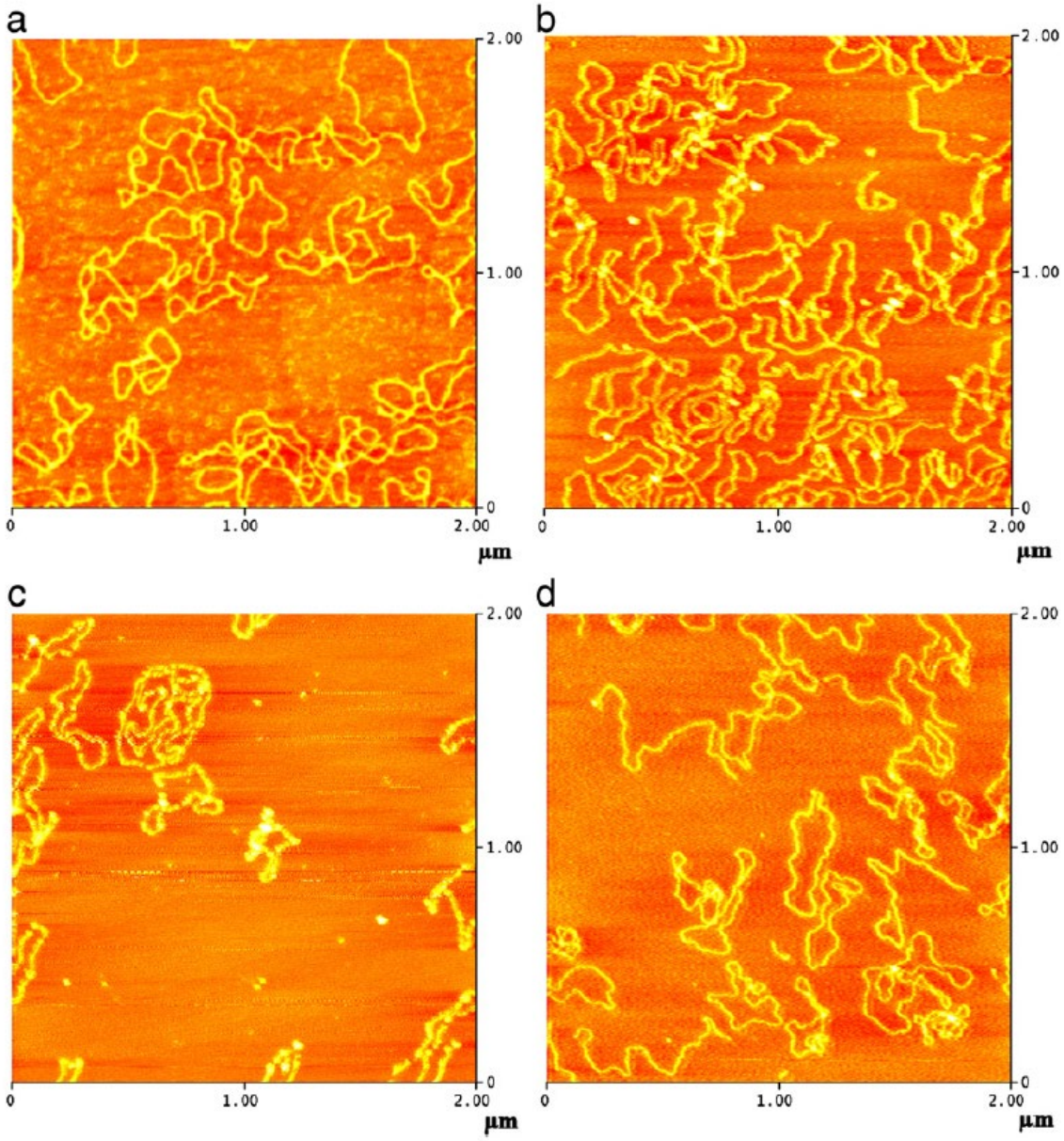

782

783

784

785

786 **Figure 4**

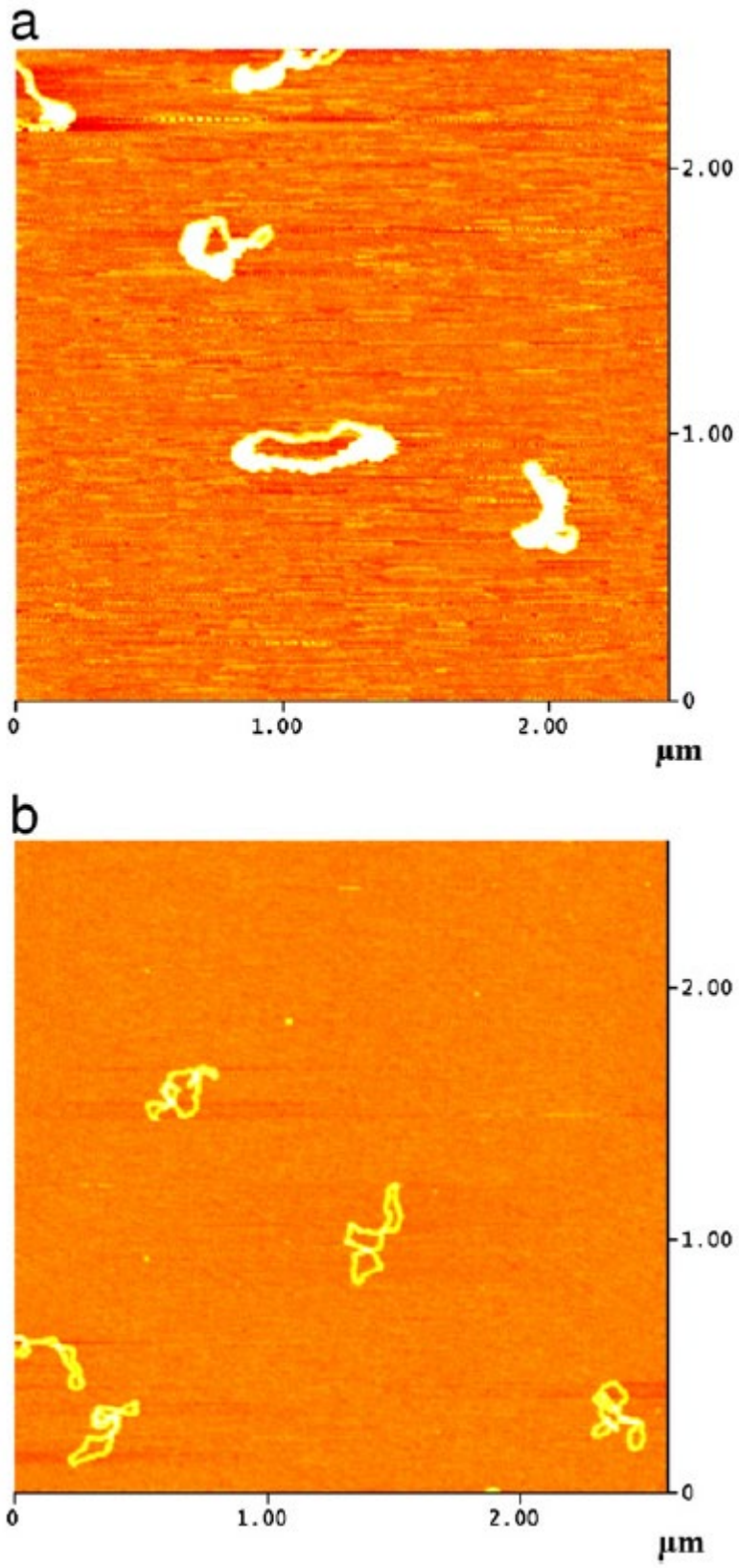

787

788

Figure 5

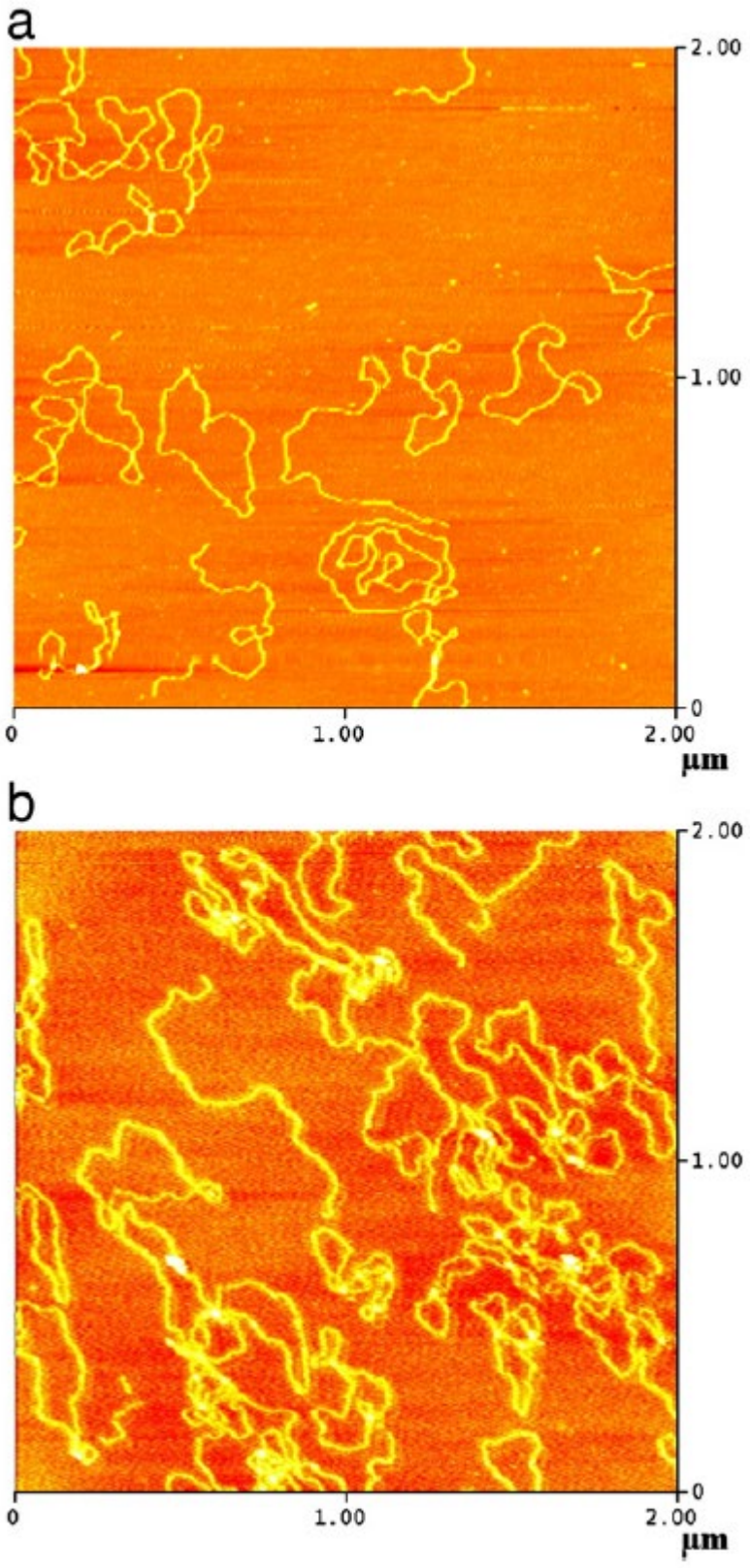

793 **Figure 6**

794

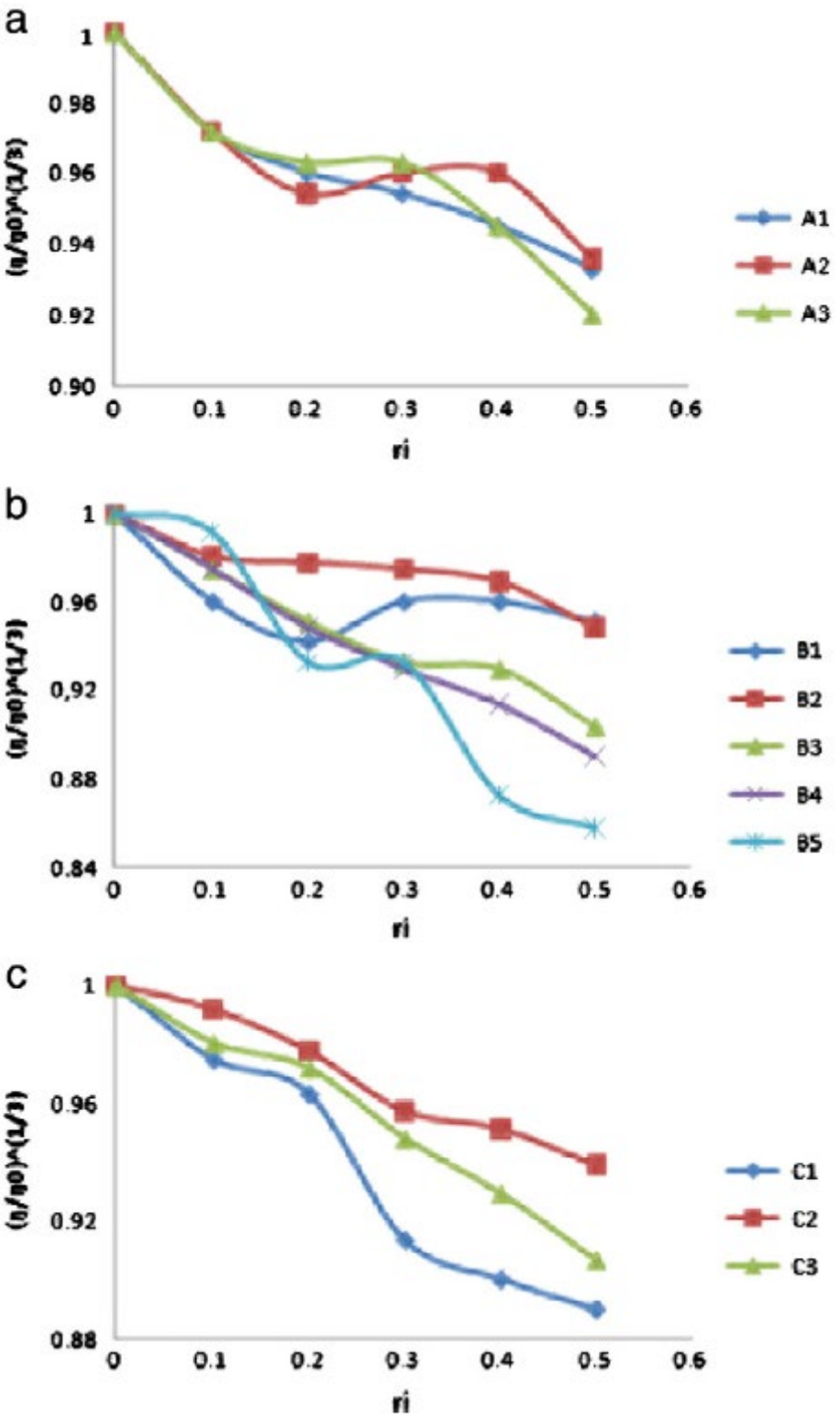

795

796

Figure 7

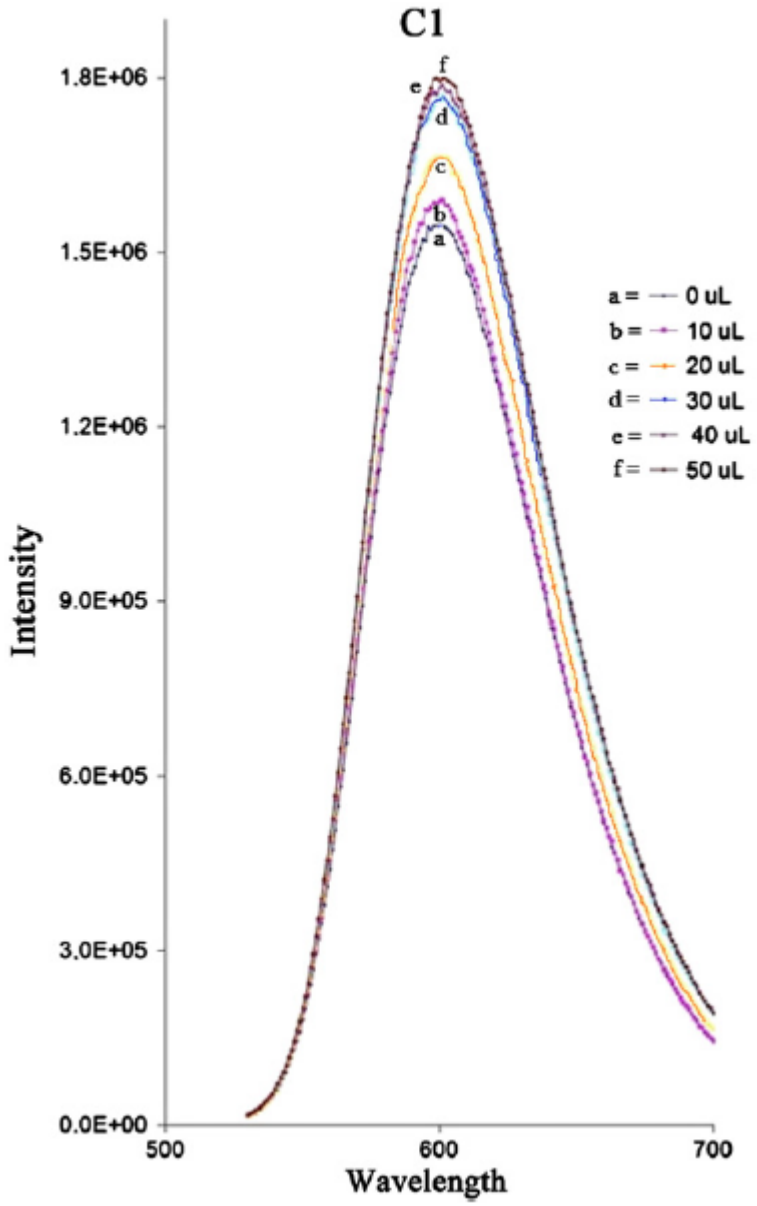
C1
1.8E+06
1.5E+06
1.2E+06
9.0E+05
6.0E+05
3.0E+05
0.0E+00
Intensity
500
600
700
Wavelength
a = 0 uL
b = 10 uL
c = 20 uL
d = 30 uL
e = 40 uL
f = 50 uL